PREDICTION OF SHRINKAGE STRESSES IN PAVEMENTS CONTAINING SOIL-CEMENT BASES

P. C. Pretorius, Bruinette, Kruger, Stoffberg and Hugo, Pretoria, South Africa; and
C. L. Monismith, Institute of Transportation and Traffic Engineering,
University of California, Berkeley

The occurrence of shrinkage cracks in pavements containing soil-cement bases is quite common. Whether such cracking is detrimental to the structural behavior of the pavement section depends on a number of factors, including environment and materials used in the pavement. The fact that problems have been experienced in some pavements subsequent to this cracking justifies an attempt to formulate an analytical procedure that would permit the prediction of shrinkage stresses and cracks in pavements containing soil-cement bases. This paper permits 1 such an approach using the creep characteristics of all of the materials in the pavement structure together with the shrinkage and strength characteristics of the soil cement in an incremental axisymmetric finite-element solution. Stresses are predicted at selected time intervals by increasing the shrinkage strains in the soil cement in small time increments and allowing relaxation due to creep to occur before superposition of the next shrinkage increment. Two cases are analyzed: one considers a uniform shrinkage in the soil cement; the other considers a differential shrinkage assuming that desiccation begins at the surface of the soil-cement base and migrates toward the interior. Also included is a brief discussion of the influence of asphalt concrete temperature and thermal effects on the magnitude of the shrinkage stresses.

•THOUSANDS of feet of cement-treated base can be constructed daily with modern construction equipment. Shrinkage is an inherent property of such a material and begins occurring soon after the material has hardened.

No shrinkage stresses will be developed for a cement-treated base constructed on a frictionless surface and subjected to uniform shrinkage strains throughout its depth. If shrinkage in the layer is restrained in any way, however (i.e., by continuity with other layers, by interlayer friction, or by differential shrinkage), stresses will be developed. In general, 1 factor or a combination of these factors will be present in the field, and the development of shrinkage stresses is, therefore, inevitable.

As these stresses develop, they may be relieved by relaxation because many materials that exhibit shrinkage also exhibit creep. Because the magnitude of shrinkage stresses is proportional to the length of a continuous base, stress relief by creep may initially be insufficient to keep the stresses below the tensile strength of the material, in which case cracking of the cement-bound material will occur. This cracking may be accompanied by an elastic recovery with a corresponding reduction in shrinkage stress. Shrinkage continues, however, and the process keeps repeating itself until the resulting stresses do not exceed the tensile strength of the material.

This is a difficult problem to analyze mathematically, but a method of analysis appears desirable if a better understanding of the factors that influence shrinkage cracking in cement-treated materials is to be achieved. Many authorities disagree as to whether such cracking is really a problem. Recent South African experience (1), for

Sponsored by Committee on Theory of Pavement Design and presented at the 50th Annual Meeting.

example, justifies such an investigation because the formation of wide shrinkage cracks allowed water infiltration that weakened the subgrade and led to severe fatigue cracking in the pavement structure.

It is possible today to analyze this problem, at least to a first approximation, by using the finite-element method. It is possible not only to consider different material characteristics in each element but also to effectively treat nonlinear problems with a step-by-step linear incremental procedure or with interaction (2). The development of shrinkage stresses can be analyzed similarly by incrementing the shrinkage strains in small time intervals and by allowing creep relaxation to occur after each shrinkage increment until the maximum shrinkage has been achieved or until cracking has occurred. The process of elastic recovery after cracking complicates the analytical treatment of the problem considerably, and simplifications have to be introduced.

Shrinkage cracks are usually observed the first few days after construction. These cracks are very fine, but this early crack spacing may be very close to that finally obtained. Accordingly, an approach would be to assume a crack spacing and analyze the pavement to predict whether further cracking will occur. By repeating this procedure, a final crack spacing (and crack width) can be estimated. Stress relief at cracking is ignored by this approach, and, although it will be shown that precise values of stress are not determinable at the moment because of a number of uncertainties in the analysis, it will be possible to show the relative importance of the factors that control the development of shrinkage stresses in a pavement.

From the discussion in the foregoing, it follows that a proper analysis requires the shrinkage, creep, and strength characteristics of the cement-treated material as well as similar properties for the other layers present in the pavement.

For the present investigation, a 3-layer pavement was selected consisting of a 3-in. asphalt concrete layer overlaying an 8-in. soil-cement base (according to the Portland Cement Association definition of soil cement) resting on a clayey subgrade. Properties of the cement-treated material were determined experimentally, whereas appropriate properties for the other materials were obtained from other test programs in which similar materials had been used.

Figure 1 shows a complete subsystem for the analysis of a pavement and one that considers shrinkage and creep as well as thermal effects and loading. In this paper, only the lower portion of the subsystem shown in Figure 1 will be described. The com-

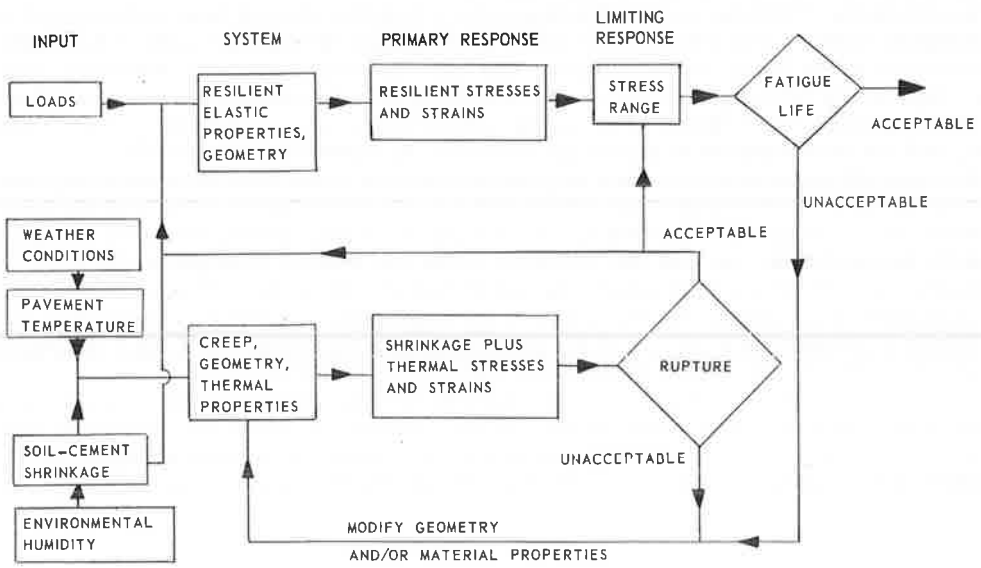

Figure 1. Design subsystem considering shrinkage and creep.

plete subsystem, including loading effects, is important for design consideration and has been treated in detail elsewhere (22).

MATERIAL PROPERTIES

Soil-Cement Base

Materials—The aggregate used in this investigation consisted of a partially crushed gravel obtained in fractions of 2 sizes (designated A and B, Fig. 2) and silty clay (C, Fig. 2) combined in the proportion 4A:1B:1C (Fig. 2) to produce a material designated A-2-4, according to the AASHO classification. The silty clay (3) exhibited the following characteristics: liquid limit, 29.2 percent; plastic limit, 19.4 percent; plastic index, 9.8 percent; organic content, 2.5 percent; clay mineral composition, illite and montmorillonite; and AASHO classification, A-4. A cement content, based on the Portland Cement Association wet-dry test, of 5.5 percent by weight was determined for the selected gradation.

Vibratory compaction at a water content of 7.5 percent by weight was used to prepare the laboratory specimens. Prior to compaction, the aggregate was oven-dried at 235 F for about 18 hours. Because such treatment would influence the properties of the silty clay, this material was air-dried until its water content was reduced to a level less than 2 percent.

Uniform mixtures were obtained by separating the aggregate into a series of sizes and then by recombining them to meet the grading shown in Figure 2. The graded aggregate and cement were thoroughly mixed in a rotating pan, after which water was added to the mixture through a nozzle under pressure. Addition of the water required 2 to 3 min. during which time mixing was continued. Immediately following mixing, the specimens were compacted as noted previously. A variation in density of less than ±2 percent about the mean (138 lb/cu ft) was obtained.

Shrinkage Properties—The magnitude and rate of shrinkage of soil cement are influenced by a variety of factors with clay content having dominant influence. Although portland cement concrete shrinks slowly and continuously and may reach a magnitude

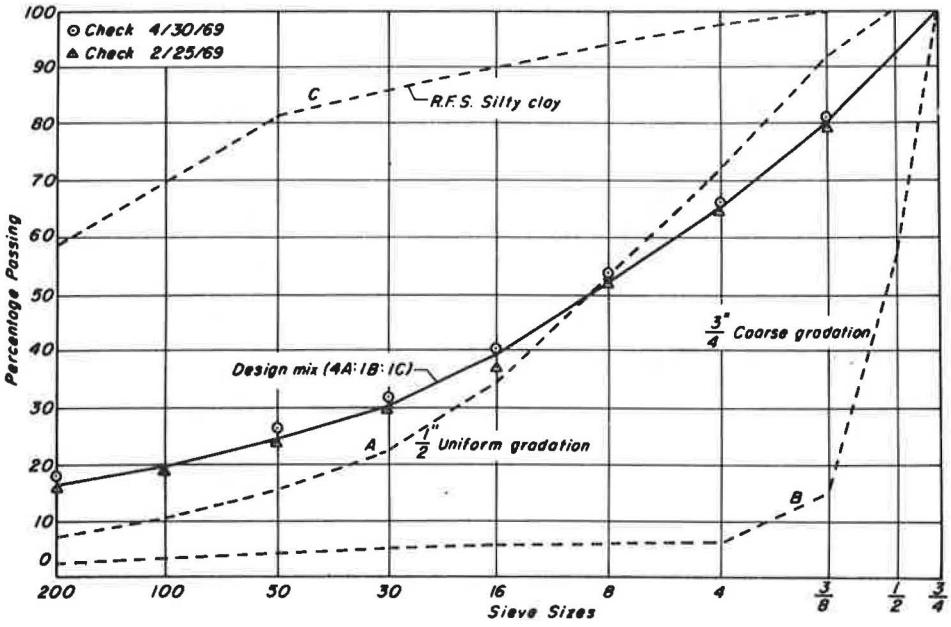

Figure 2. Distributions of grain sizes of materials used in soil-cement base.

of only 1,200 x 10^{-6} in./in. over a period of 30 years (4), soil cement can shrink as much as 2,000 x 10^{-6} in./in. in only 13 days (5).

For the soil cement under consideration, the following procedure was followed for recording shrinkage strains. Beam specimens, 3 in. square by 18 in. long, were compacted with ¼-in. diameter by 3-in. long stainless steel bolts cast 1½ in. into and perpendicular to the 3-in. square ends of the beam. The protruding points of these bolts were previously carefully rounded and served as reference points for the subsequent shrinkage measurements. Shrinkage was recorded by a vertically mounted 0.0001-in. dial gage, as is shown in Figure 3, relative to an aluminum reference beam that was insulated at handling points and stored under the same conditions as the specimens. Specimens were cured for varying periods at 100 percent relative humidity before being transferred to lower relative humidity environments. During this initial curing, little dimensional change occurred. Reductions in length on the 90, 65, and 30 percent relative humidity environments are shown in Figures 4 and 5. The data shown in Figures 4 and 5 indicate that the rate as well as the magnitude of shrinkage increases as the ambient relative humidity decreases. Also noted is the fact that prolonged moist-curing increases the shrinkage potential. This may be due to an increase in the products of hydration (and, in this respect, the behavior of the mix is similar to that of concrete).

As shown in Figures 4 and 5, most of the shrinkage occurs within the first 30 days. This high initial rate of shrinkage is probably due to the suction forces resulting from the loss of capillary water. The rate of shrinkage decreases as equilibrium is approached. In the later stages, shrinkage is more than likely caused by a loss of surface-absorbed and interlayer water (6). Figure 6 shows that a linear interpolation of shrinkage strains is possible over the range of relative humidities indicated.

For the analytical investigation, polynomials were fitted to the shrinkage data points that allowed easy interpolation for any desired time and relative humidity within the range considered.

Creep—Where the pavement layer is subjected to shrinkage under restrained conditions, creep in the layer will reduce both the rate of development and the magnitude of the resulting stresses.

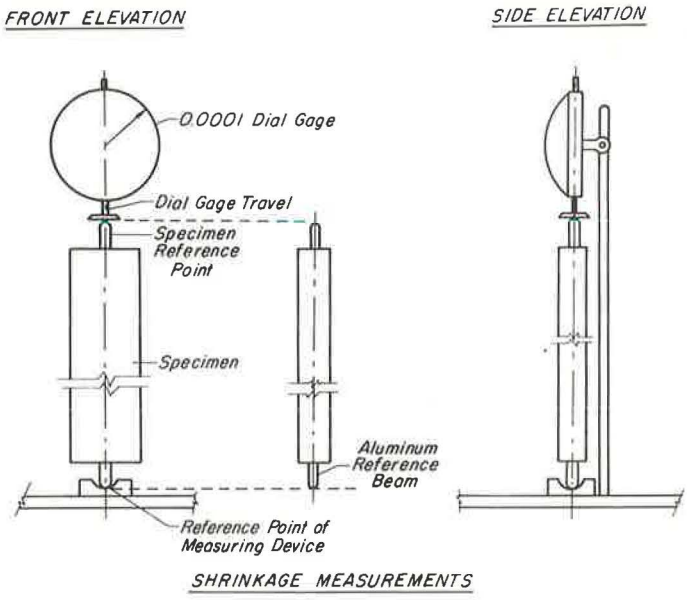

Figure 3. Equipment and specimen configuration for shrinkage measurements.

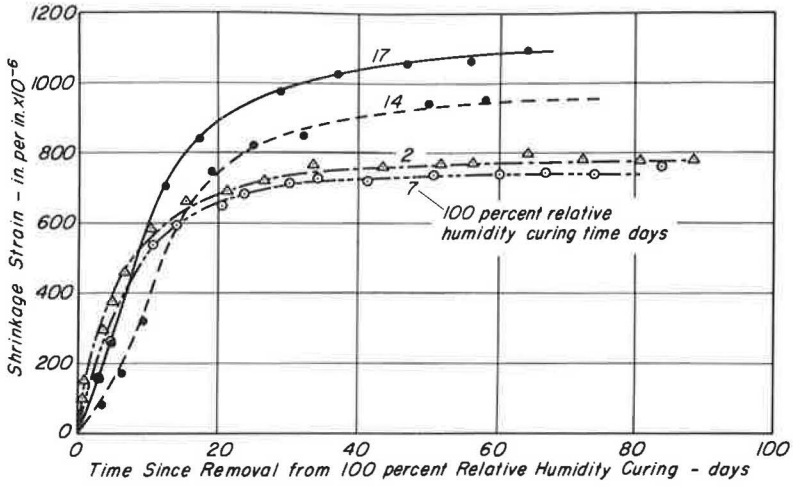

Figure 4. Shrinkage strain versus time for specimens in 30 percent relative humidity environment.

It is generally assumed that creep in tension and in compression has the same characteristics (5, 7). The usual procedure, therefore, is to determine creep in compression and apply the results to problems dealing with tension. Work by Illson (8) on concrete has indicated, however, that the rate of creep in direct tension can be much higher initially than the rate of creep in compression. If this is true for soil cement, then the stresses predicted on the basis of compression creep tests would initially be too large. Accordingly, it was decided that creep in tension would be more representative, and equipment shown in Figure 7 was developed to conduct tensile creep experiments. [Ideally, the creep experiment should be conducted in accordance with the strain gradient expected in the pavement. Because the strain gradient has a significant influence

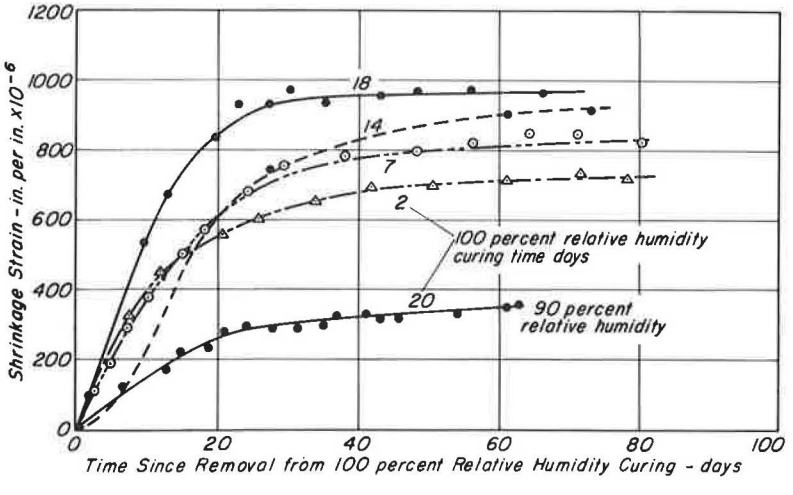

Figure 5. Shrinkage strain versus time for specimens in 65 percent and 90 percent relative humidity environments.

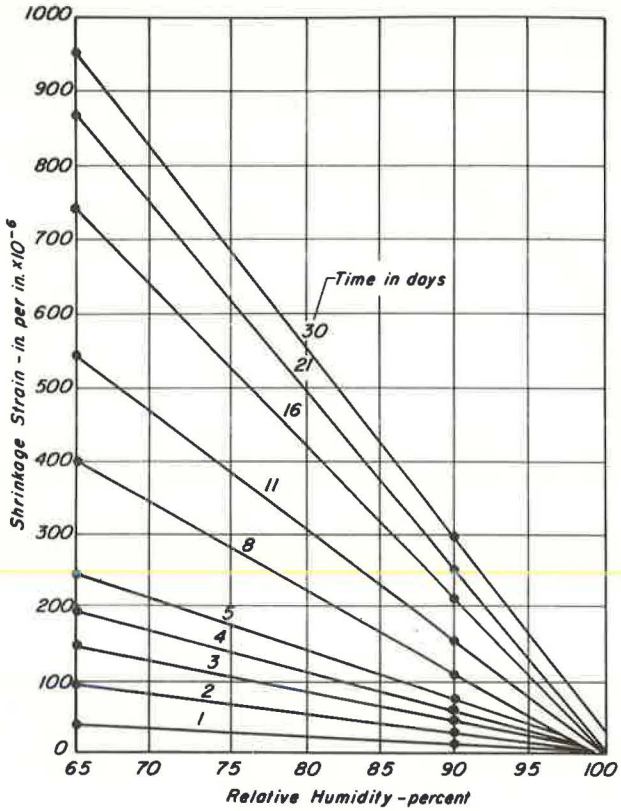

Figure 6. Influence of time on relationship of shrinkage strain and relative humidity for specimens cured initially for 17, 18, and 20 days in 100 percent relative humidity environments.

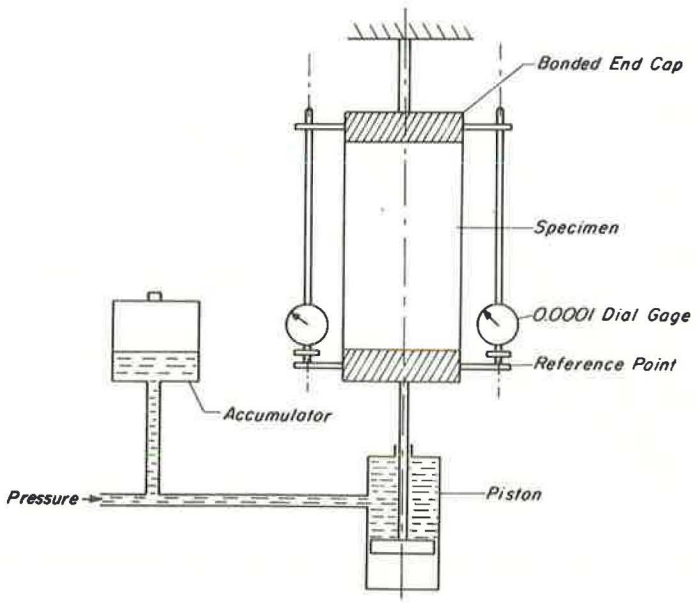

Figure 7. Creep measurement apparatus.

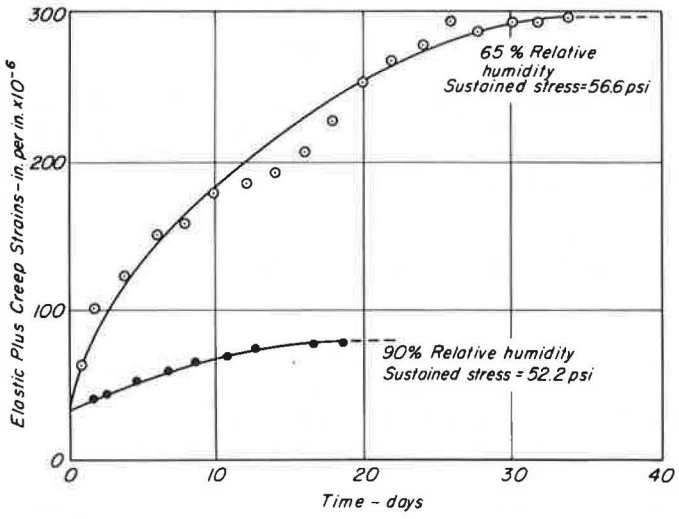

Figure 8. Creep strain versus time for specimens in 90 percent and 65 percent relative humidity environments (specimens cured initially 18 or 20 days in 100 percent relative humidity environment).

on both the strength characteristics and fatigue response of soil cement (22), it can be expected to influence creep behavior. Thus, direct tension creep tests would be applicable, strictly speaking, to uniform shrinkage problems only.]

It should be noted that there are a number of problems associated with tension creep testing of soil cement. For example, the stress level must be comparatively small to ensure that the material will not fail with time (7, 9). Because the tensile strengths of cement-treated materials are comparatively low, the stresses to be applied in creep are correspondingly smaller, with the results that small creep strains are obtained. This in turn necessitates that careful measurements be made. The procedure by which this was accomplished is shown in Figure 7. Resulting creep data are shown in Figure 8. It will be noted in Figure 8 that the creep response of the material is similar to its shrinkage behavior (Figs. 4 and 5). The rate and magnitude of creep increase as ambient humidity is reduced, and the major portion of the creep strain occurs within the first 30 days.

In the finite-element analysis used here, stiffness rather than creep characteristics are required. Ideally, the stiffness characteristics should be determined by means of a relaxation test. In this type of test, the strain ϵ_0 is kept constant while the change in stress $\sigma(t)$ with time is recorded. The relaxation modulus $E(t)$ is then defined as

$$E(t) = \frac{\sigma(t)}{\epsilon_0}$$

Such tests are extremely difficult to perform, and the usual procedure is to conduct creep tests and derive a relaxation modulus from these results. At least 2 procedures are available to make this determination. The first procedure involves the direct inversion of the creep compliance:

$$D(t) = \frac{\epsilon(t)}{\sigma_0}$$

where σ_0 = applied constant stress and $\epsilon(t)$ = strain varying with time, to yield a relaxation modulus

$$E(t) = \frac{\sigma_o}{\epsilon(t)}$$

This modulus is sometimes referred to as the reduced stiffness. Direct inversion may not necessarily produce a correct time-dependent modulus. Accordingly, a second procedure is to assume that the material is linearly viscoelastic in response and, thus, that the following superposition relation is applicable:

$$\int_0^t E(t)\, D(t - \tau)\, d\tau = \int_0^t E(t - \tau)\, D(t)\, d\tau = 1$$

This equation makes it possible to solve for 1 function (e.g., the modulus) if the other (i.e., the compliance) is defined on the time scale. Hopkins and Hamming (10) developed a technique to solve this equation by numerical means, whereas Monismith, Alexander, and Secor (11) successfully applied it to test data on asphalt concrete.

Both procedures were used to estimate the relaxation moduli from the creep data shown in Figure 8. The resulting relationships are shown in Figure 9. For use in subsequent calculations, polynomial expressions were used to represent the curves shown in Figure 9.

Because only 2 relative humidities were considered, it was necessary to develop a procedure for determining response at other humidity conditions. Based on the similarity between creep and shrinkage responses, it was assumed that linear interpolation over the relative humidity range considered was again justified. A check on reduced stiffness values determined from creep data for concrete (12) lent support to this decision.

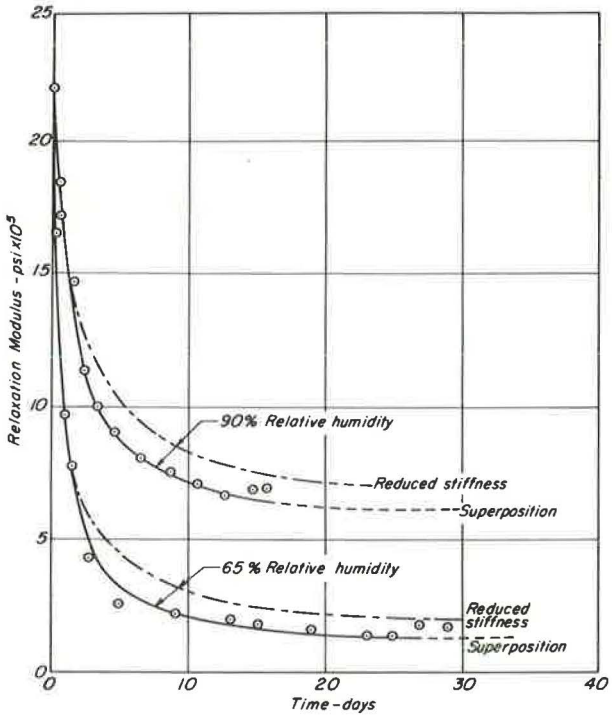

Figure 9. Relaxation moduli versus time for specimens in 90 percent and 65 percent relative humidity environments.

Strength—There are many factors that influence the strength of cement-treated materials, and a general failure criterion awaits the results of additional studies. A series of strength tests were conducted on the material used in this investigation, and the results, together with their significance, are presented in this section.

One measure of strength that is frequently used is the unconfined compressive strength. The influence of curing time on ultimate compressive strength of 4-in. diameter by 8-in. high specimens, cured under 100 percent relative humidity conditions, is shown in Figure 10.

Extensive research is being conducted on the fracture of concrete. Because many of these principles are also applicable to soil cement, they are referred to in this paper where applicable.

Shah and Winter (13) traced the nonlinear behavior of concrete to the mortar-aggregate interface that constitutes the dominant weak link in a mix. Shah and Chandra (14) related the internal microcracking and crack propagation to the external parameters of volume change and Poisson's ratio. Variation of these parameters with stress level expressed as a percentage of the unconfined compressive strength (Fig. 10) is shown in Figure 11 for the soil cement.

The initiation stress σ_i, the stress at which Poisson's ratio begins to increase, is an indication of a beginning in significant bond cracking; i.e., cracking of the mortar-aggregate interface. At the critical stress σ_{CR}, these bond cracks are bridged by mortar cracks, and the specimen begins dilating. Below σ_i, linearity in the stress-strain relationship exists.

Direct tensile strength and modulus of rupture tests were also performed. The direct tensile strength tests were conducted on specimens 4 in. in diameter by 8 in. high with load-transfer end caps bonded to each specimen with epoxy resin. Modulus of rupture tests were performed by using third-point loading on beams 15 in. in length with a 3-in. square cross section. The results are shown in Figure 12.

These results indicate that the strain gradient has a significant influence on the tensile strength of the material. Although the strain gradient is zero for a direct tensile test, it is constant in a flexural experiment. The strength in a splitting tensile test, with yet another strain distribution, is somewhere between these 2 values (15).

Materials in the pavement section are seldom subjected to only uniaxial stresses. The presence of any or both of the other principal stresses may modify the strength characteristics substantially. Figure 13 shows the influence of confining pressure on the compressive strength and stress-strain relationship of the soil cement. Confinement increases the strength significantly and also makes the material more ductile. Figure 13 also shows that curing increases the brittleness during unconfined compressive strength testing.

Of the many failure criteria for combined stresses that are available, the distortion energy theory of Van Mises would appear to hold most promise for concrete-like ma-

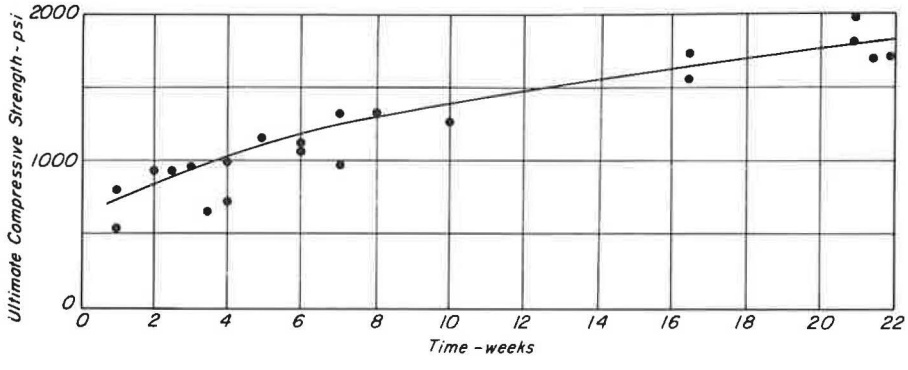

Figure 10. Relationship between unconfined compressive strength and time for soil cement.

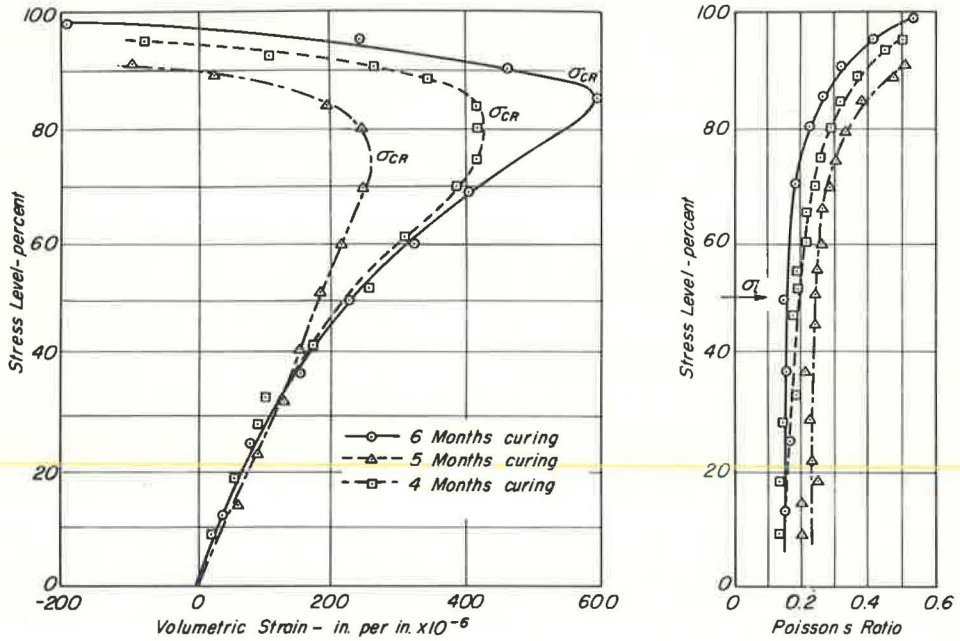

Figure 11. Influence of stress level on volumetric strain and Poisson's ratio for soil-cement specimens.

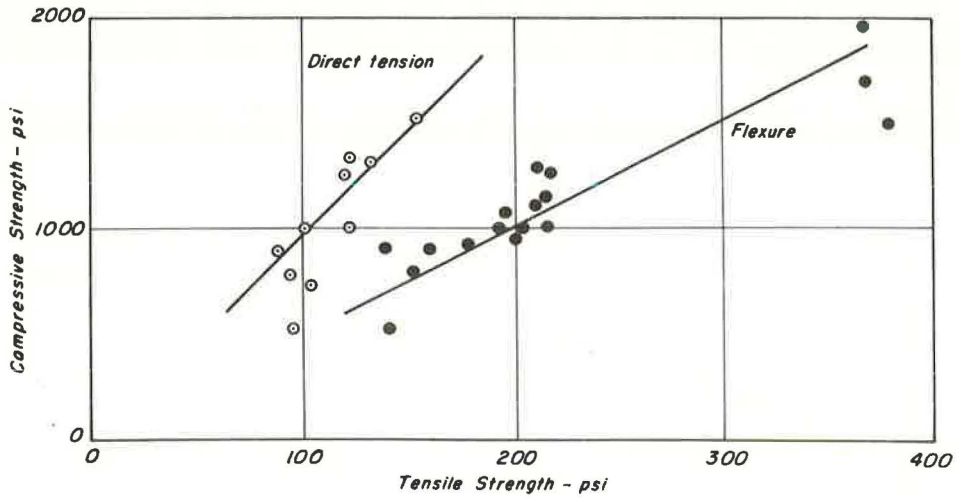

Figure 12. Relationships between tensile strength and unconfined compressive strength for soil-cement specimens.

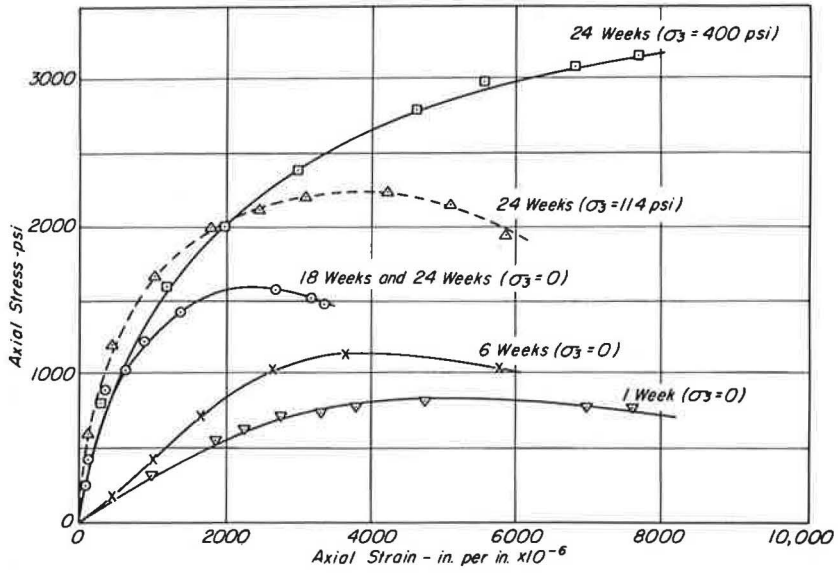

Figure 13. Typical stress versus strain relationships in triaxial compression for soil-cement specimens.

terials. According to this theory, the failure surface, in terms of octahedral stresses, is expressed by

$$\tau_o = a + b\,\sigma_o$$

where

τ_o = octahedral shearing stress = $\frac{1}{3}\,(\sigma_1 - \sigma_2)^2 + (\sigma_2 - \sigma_3)^2 + (\sigma_3 - \sigma_1)^2$,
σ_o = octahedral normal stresses = $\frac{1}{3}\,(\sigma_1 + \sigma_2 + \sigma_3)$, and
a and b = constants.

This approach has produced fair results in biaxial compression-tension tests for concrete (16, 17). Recently, Kupfer, Hilsdorf, and Rusch (18) conducted biaxial strength tests under all combinations of load for concrete. From the results presented, it was possible to plot data shown in Figure 14 in terms of octahedral stresses. It is clear that 1 linear expression is not sufficient to define the total failure envelope. It is possible, however, to define a failure criterion in the compression-tension zone, for example, by conducting only 2 tests—an unconfined compression strength test and an unconfined tensile strength test. For the soil cement, this approach yielded the following equation:

$$\tau_o/\sigma_c = 0.08571 + 1.157\,(\sigma_o/\sigma_c)$$

which is not much different from that developed by Kupfer, Hilsdorf, and Rusch (18) for concrete (Fig. 14) or the equations presented by McHenry and Karni (17) and Bresher and Pister (16). It should be noted that the confined compression test results for the soil cement showed a very distinct nonlinear deviation from the straight-line expression presented in the foregoing.

It is evident, therefore, that no simple failure criterion exists, even for the simple cases of uniaxial and biaxial stresses. For the problem of sustained shrinkage stresses in a pavement, the problem is complicated further by the presence of 2 additional factors; i.e., drying out of the specimen and sustained loading.

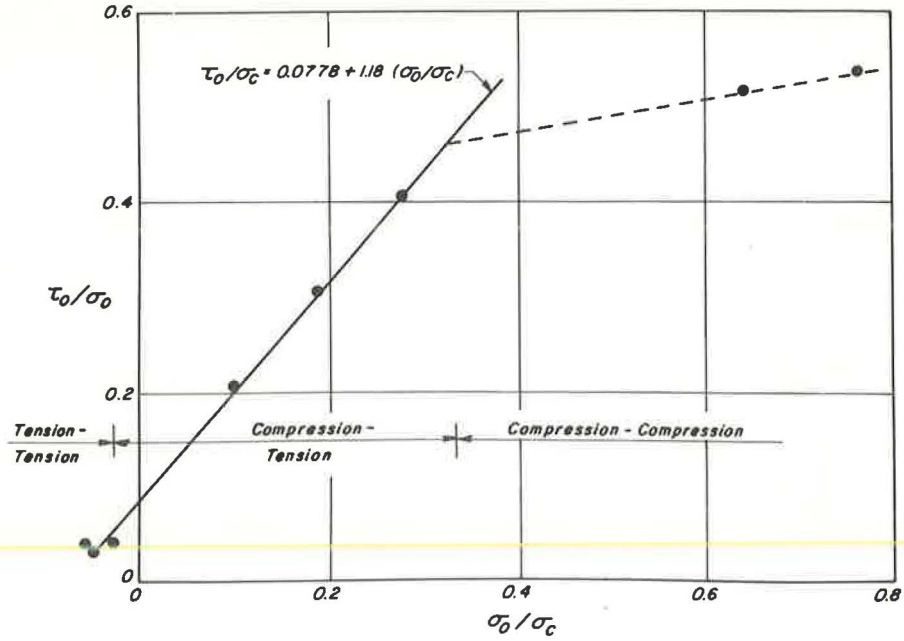

Figure 14. Results of triaxial strength tests for plain concrete (18).

A material that is shrinking is also drying, and it would be expected that drying would influence the properties of the material. In Figure 15 the influence of relative humidity on the direct tensile strength of soil cement is shown. Where a 100 percent relative humidity environment caused a steady increase in strength, lower relative

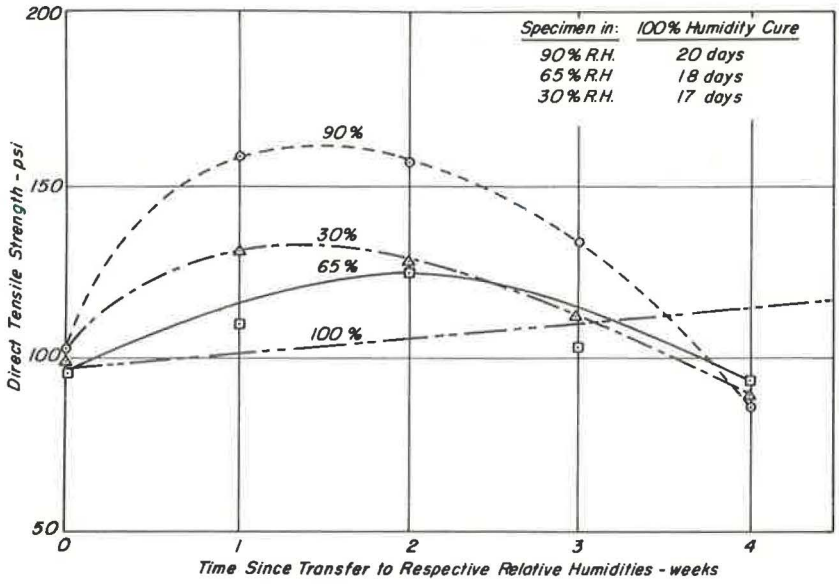

Figure 15. Influence of curing in different humidity environments on ultimate tensile strength of soil-cement specimens.

humidities had the effect of contributing initially to an increase in strength and then to a marked reduction. The same effect was noticed on the secant modulus of elasticity.

Figure 16 shows the effect of the initial curing period on the modulus of rupture after a prolonged period of drying. In Figure 16, the following is noted:

1. The strength increases with the time of initial curing;
2. Flexural strengths of specimens subjected to drying are independent of the relative humidity that caused the dried-out condition; and
3. Little difference in strength exists for specimens cured for periods longer than 20 days as compared to those cured continuously.

In general, if a material is subjected to a sustained load, failure will occur after some time if the sustained load is large relative to the short-term strength. Studies of concrete by Meyers, Slate, and Winter (9) indicate that mortar cracks should not result upon application of the sustained load if time failure is to be prevented; i.e., the stress should be below the critical stress σ_{CR}. For soil cement, this corresponds to a mean stress level as low as 75 percent (Fig. 11).

States of stress in the problem under consideration here are predominantly biaxial tension versus tension subjected to a significant strain gradient. Under such conditions, the uniaxial direct tensile strength or modulus of rupture (depending on the strain gradient) are acceptable failure criteria, and little advantage is gained, at the moment, by additional testing effort. Because of the sustained nature of the loading, failure would occur at a certain percentage of these values.

Asphalt Concrete

In the analysis presented here, the only property required for the asphalt concrete is its creep response. Rather than developing such data, we used stiffness characteristics for an asphalt concrete developed by Pagen (19). These characteristics, represented by a creep modulus, are shown for an extended time scale at 25 C (298 K). The corresponding temperature-dependent shift factor a_t is shown in Figure 17. It will be noted in Figure 18 that the modulus remains fairly constant (approximately equal to 10,000 psi) for temperatures above 40 F and relaxation times longer than about 1 day.

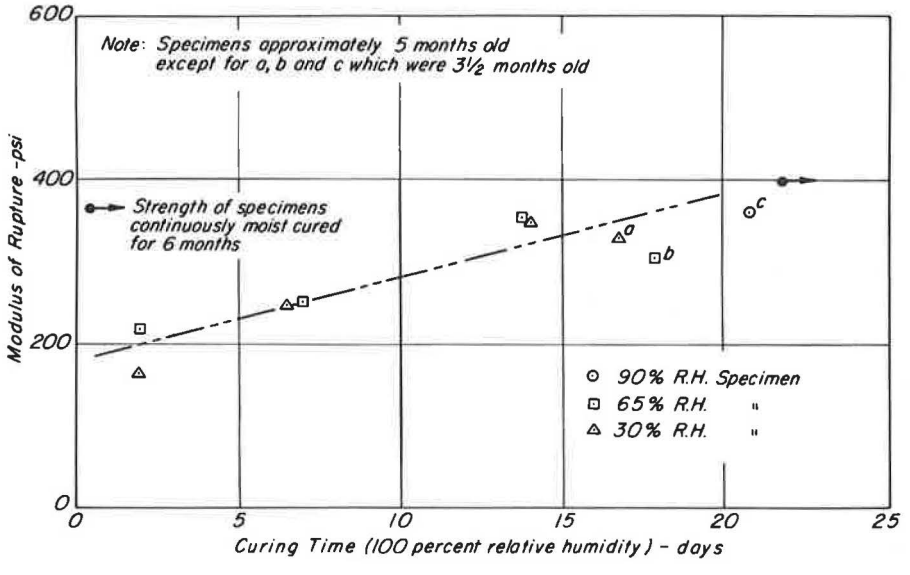

Figure 16. Influence of initial curing period on modulus of rupture of soil-cement specimens after prolonged drying period.

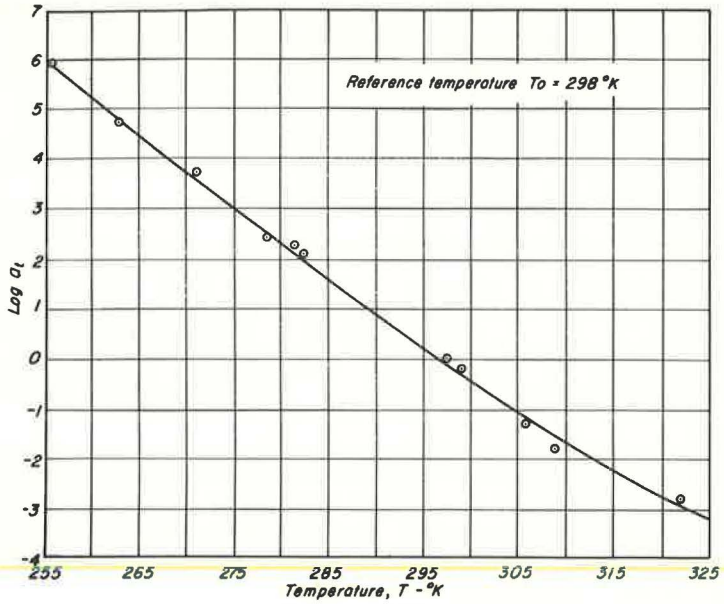

Figure 17. Influence of temperature on shift factor a_T for asphalt concrete (19).

Clayey Subgrade

Based on research conducted by Paduana (20), it was decided to use a constant modulus of 1,500 psi for the clayey subgrade because his data indicated that materials of this type reached an equilibrium value in creep fairly rapidly.

ANALYTICAL INVESTIGATION

An outline of the finite-element approach to the problem is given in the Appendix. By this approach the element nodal points are locked, and the required nodal forces

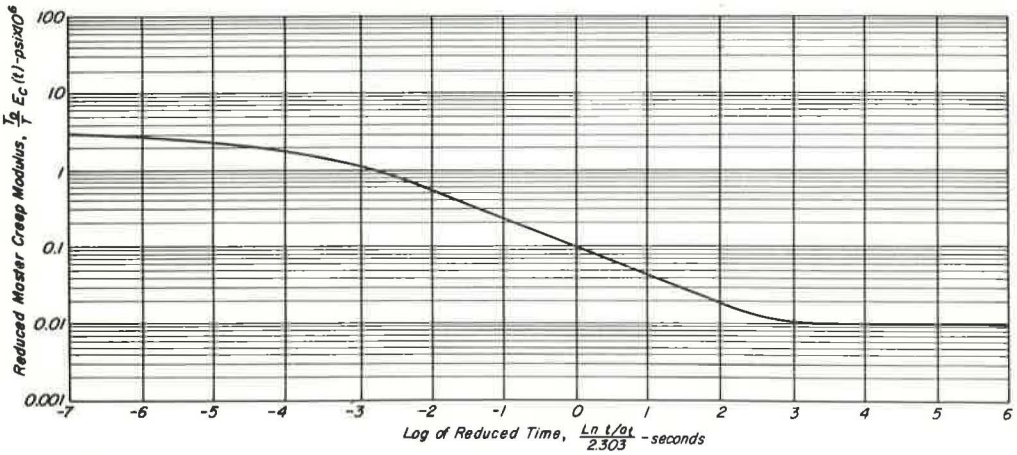

Figure 18. Composite creep curve for asphalt concrete (19).

are determined for a finite increase in shrinkage strains. These nodal forces are then reversed, applied to the system, and solved for stresses and displacements. The final stresses are obtained by a superposition of the stresses due to full restraint and the stresses due to nodal point displacements. This procedure is followed for each strain increment, and the stresses are added to those calculated in the previous increments. Relaxation due to creep is taken care of at each time increment by using the relaxation modulus corresponding to the difference in time between the final time and the time of increment.

This problem ideally should be treated with a 3-dimensional finite-element approach. Such programs currently require too much computer time to be of practical use. The other alternatives are axisymmetric, plane stress, or plane strain idealizations of the problem. Initially, before cracking occurs, a plane stress approach seems appropriate; but, after the pavement has cracked into smaller, more or less rectangular blocks, an axisymmetric idealization would appear to be the best approach. Accordingly, a constant strain axisymmetric finite-element program was used for this analysis.

In the analysis, the following assumptions were made:

1. Linear viscoelasticity is applicable to failure.
2. Continuity exists between all layers.
3. The experimental data presented here are applicable. It should be noted that laboratory creep and shrinkage results to be used in the analysis were obtained from specimens that had been cured 3 weeks prior to testing. In the field, shrinkage and creep begin almost immediately after construction, and it is not known what effect the presence of an asphalt concrete layer would have on shrinkage in the soil cement.
4. A crack penetrates the asphalt concrete to its full depth immediately and also to some depth into the subgrade. If continuity between layers did exist and a cement-treated base did crack, the layers in contact with the cement-bound material would also have to crack with it at the interface because 2 points adjacent to the crack with 0 distance between them are suddenly given a finite displacement. Even if continuity were destroyed over a certain distance, high stresses would still be developed for shrinkage after only 1 day, as shown in Figure 19. Figure 20 shows the axisymmetric finite-element mesh assumed for subsequent analysis with a crack spacing at 20 ft. The ele-

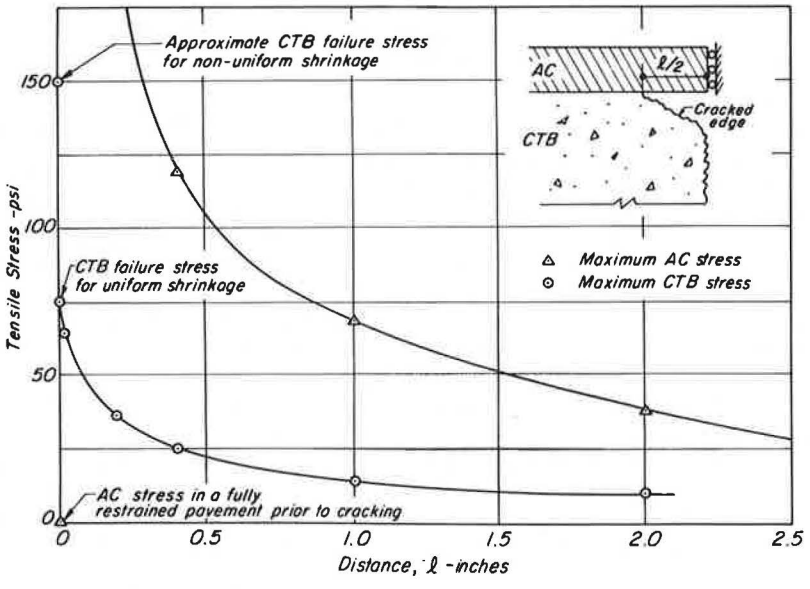

Figure 19. Influence of lack of continuity between layers on tensile stresses in asphalt-bound and soil-cement layers due to 1-day shrinkage at 65 percent relative humidity.

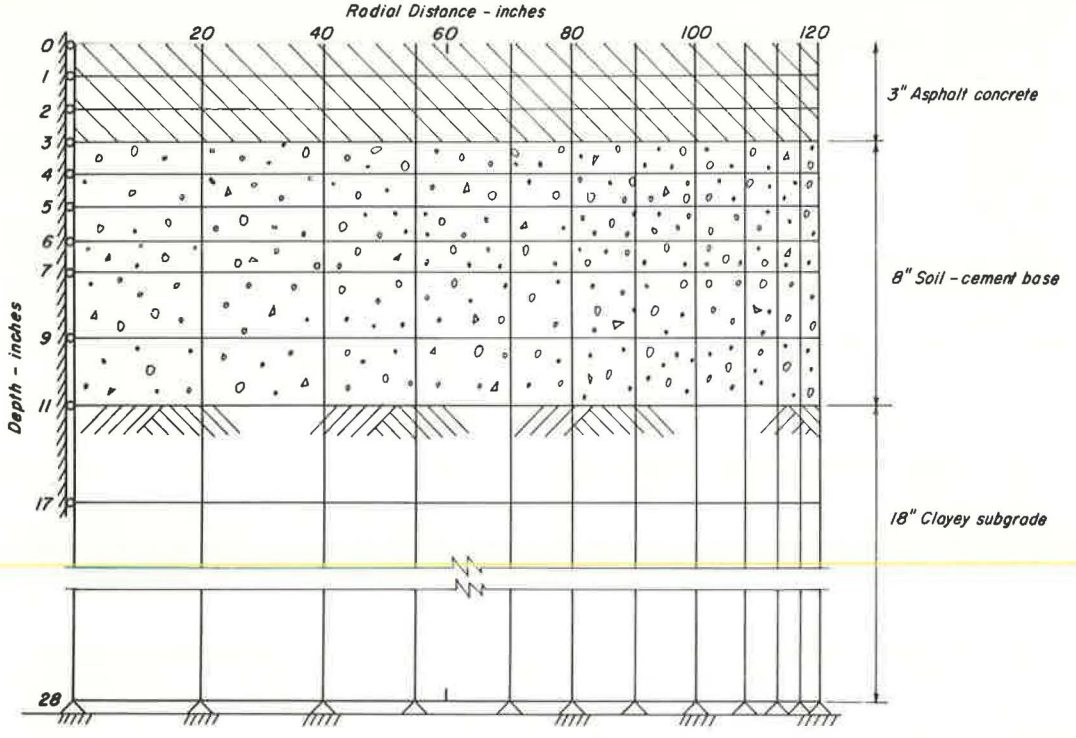

Figure 20. Finite-element representation of pavement structure for shrinkage stress determinations.

ment configuration was arrived at after some experimentation to ensure acceptable a curacy for a reasonable solution time on the computer of about 30 sec per shrinkage increment.

5. Temperatures in the asphalt concrete were varied from 87 to 50 F through its depth. Data on temperature distributions in a 2.5-in. thick asphalt layer for a pavement near Morro Bay, California, developed by Kasianchuk (21) served as a basis for this distribution.

If a pavement is subjected to a uniform shrinkage with depth, the magnitude of developed stresses depends solely on the restraint offered by the other layers. This can be regarded as a lower bound solution to the shrinkage problem.

For the pavement shown in Figure 20 subjected to uniform shrinkage, the maximum tensile stress variation with time is shown in Figure 21. These stresses are extremely small and can hardly be responsible for the final crack spacings. Factors such as thickness of asphalt concrete and its temperature have an influence on the magnitude of stresses. However, these factors are of minor importance if thermal stresses are superimposed on the uniform shrinkage stresses as seen in Figure 22. Here it is assumed that the stress-free temperature is 50 F.

It is doubtful, however, whether uniform shrinkage will ever occur in a pavement. Desiccation will probably start at the surface and migrate slowly toward the interior. One approach to this problem is to assume that the base is subjected to a parabolic distribution of relative humidity. Figure 23 shows the resulting stresses that could be developed. From the magnitude of the stresses (as compared with those shown in Figure 21), it is apparent that differential shrinkage represents a much more critical stress situation.

If the relative humidity difference between top and bottom surfaces of the cement-treated base remains fixed with time, stresses will increase at an increasing rate because the corresponding shrinkage strain difference continues to increase at an increasing rate. These stress variations are shown in Figure 24.

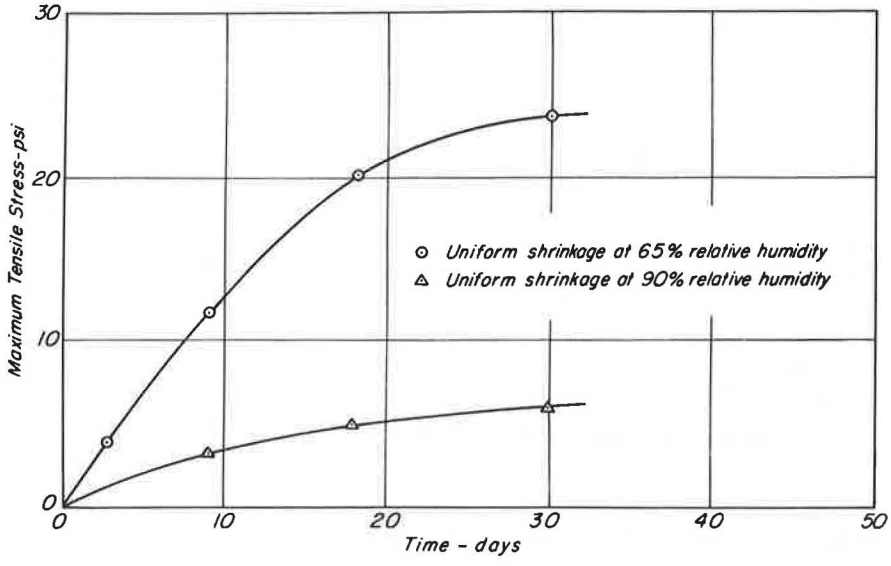

Figure 21. Development of stresses in soil-cement base resulting from uniform shrinkage (3-day strain increments).

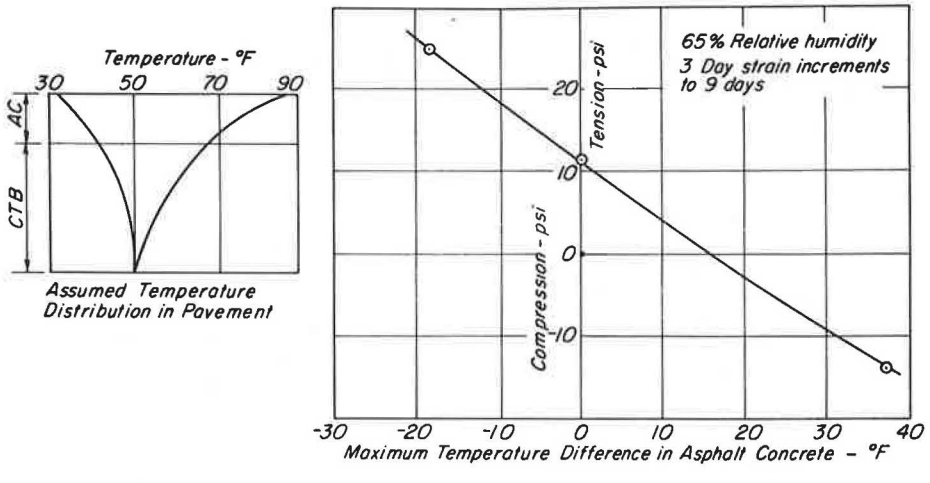

Figure 22. Superposition of shrinkage stresses for uniform shrinkage (see Fig. 21) and thermal stresses (stress-free condition at 50 F).

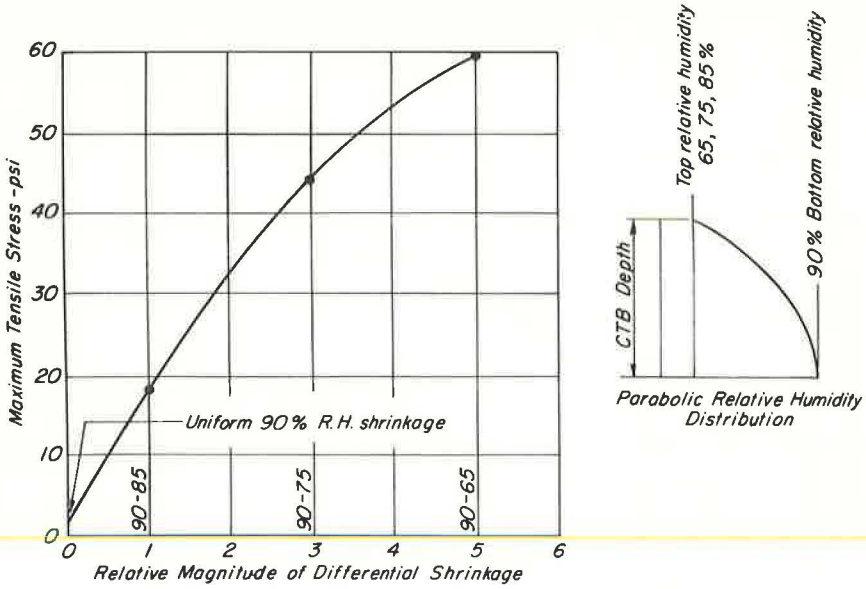

Figure 23. Influence of relative humidity distribution in soil-cement base on tensile stresses due to shrinkage.

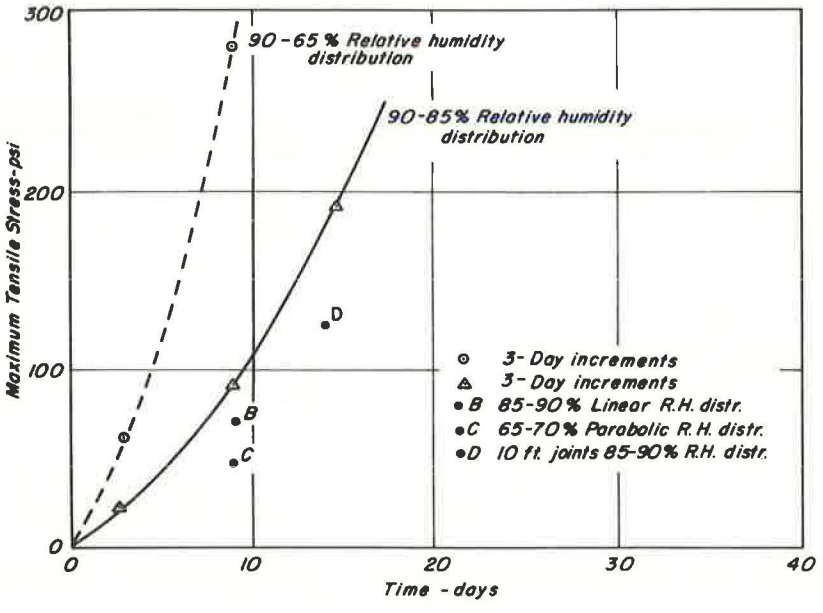

Figure 24. Influence of time on tensile stresses due to shrinkage for specific relative humidity distributions in soil-cement base.

In an actual pavement, the initial difference between the relative humidities at the top and bottom of the layer will diminish with time, until eventually the pavement will again arrive at a uniform relative humidity condition with stresses corresponding accordingly. In a finite-element analysis, this means that a redistribution of stresses is required after each strain increment to account for the diminishing differential shrinkage. Because of the uncertainties regarding the actual relative humidity distribution and rate of desiccation, as well as the extra effort and computer time required for such an analysis, this type of solution was not attempted. Instead, a rate of desiccation was assumed, and the analysis was performed without doing the stress redistribution. The resulting solution then represents an upper bound for the problem. If the lower bound solution is also known (uniform shrinkage case), an approximate solution can be obtained by simply fitting a line between the 2 extreme solutions. This approach is shown in Figures 25, 26, and 27.

Figure 25 shows the assumed humidity distributions with depth as well as with time, whereas Figures 26 and 27 indicate the results due to 2 different 5 percent humidity differentials. From the latter 2 curves, the following observations are made:

1. The band between the 2 bounds is much narrower for the 70 to 65 percent differential than for the 90 to 85 percent differential although the strains involved are exactly

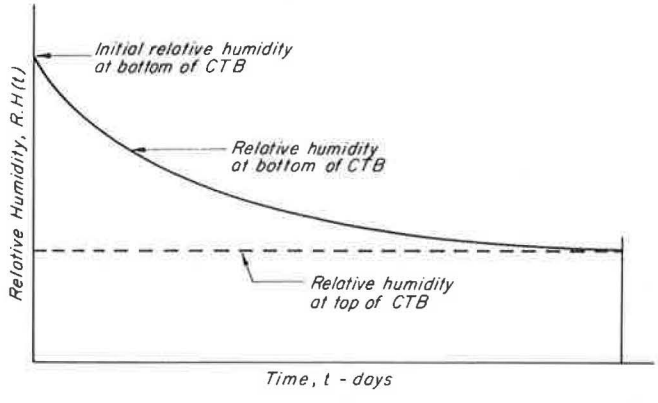

a. Relative Humidity vs. Time.

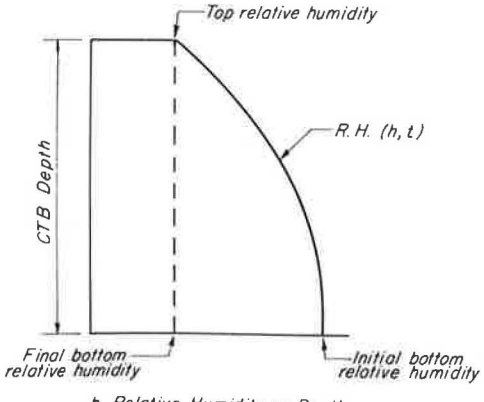

b. Relative Humidity vs. Depth.

Figure 25. Assumed time and depth variations in relative humidity for use in analyses shown in Figures 26 and 27.

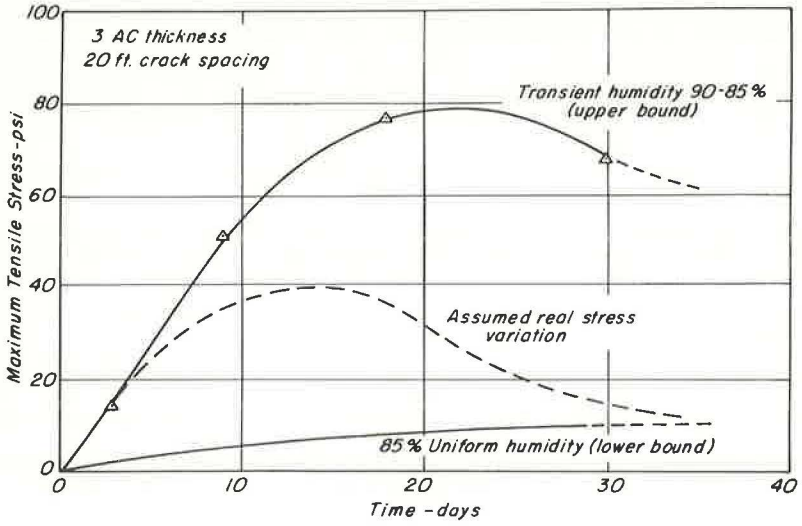

Figure 26. Variation of shrinkage stresses with time, 90 to 85 percent relative humidity differential.

the same (because of linear interpolation). This is probably due to the fact that less stress relief occurs at the higher humidities (Fig. 8), which is reflected in the higher upper bound.

2. The maximum differential shrinkage stresses are reached before the shrinkage strains reach a maximum, i.e., the shrinkage curves alone are not an indication of stress development.

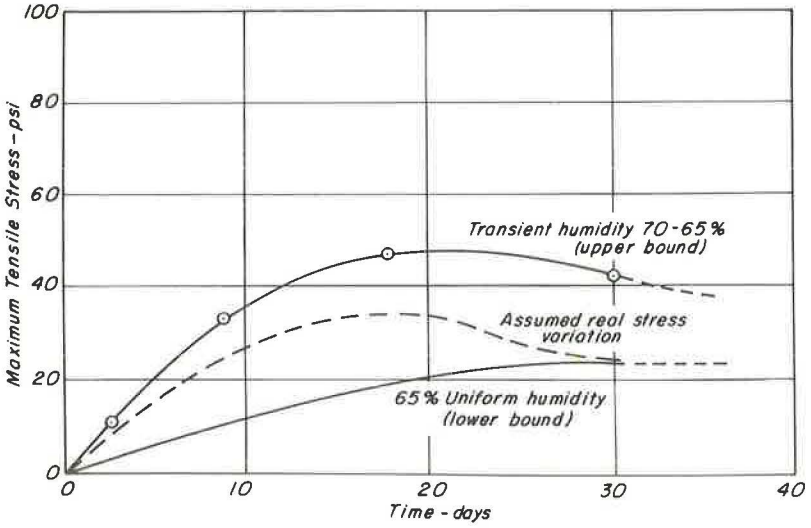

Figure 27. Variation of shrinkage stresses with time, 70 to 65 percent relative humidity differential.

SUMMARY

The results presented in this paper indicate that it is possible to approximate the crack spacing in a pavement containing a soil-cement base, provided that the actual distribution of shrinkage strains in the pavement is known. Because nodal point displacements are part of the computer output, it is also possible to predict crack widths. It is doubtful, however, that this is of significance.

Repeated loading of vehicles crossing a crack will slowly destroy any remaining friction and aggregate interlock after cracking. It is this loss of load transfer across the shrinkage crack that gives rise to fatigue cracking in the cement-bound material, and it is possible to predict the development of such distress by a 3-dimensional finite-element approach (22).

It is hoped that the approach described here or a similar approach would be applied to other types of soil-cement mixes to permit comparisons to be made. It also seems desirable that the problem of load transfer across the crack be thoroughly studied to assist in developing improved utilization of cement-stabilized soils in pavement construction.

ACKNOWLEDGMENT

This study was made possible through grants by the Portland Cement Association and the South African Council for Scientific and Industrial Research. Computer time was provided by the Computer Center, University of California, Berkeley. C. K. Chan provided valuable guidance in the design of equipment that was constructed by the shop staff of the Institute of Transportation and Traffic Engineering, University of California, Berkeley.

REFERENCES

1. Williams, A. A. B., and Dehlen, G. L. The Performance of Full-Scale Base and Surfacing Experiments on National Route 3-1, at Key Ridge, After the First Six Years. First Conf. on Asphalt Pavements for Southern Africa, Durban, Aug. 1969.
2. Duncan, J. M., Monismith, C. L., and Wilson, E. L. Finite Element Analysis of Pavements. Highway Research Record 228, 1968, pp. 18-33.
3. Wang, M. C. Stresses and Deflections in Cement-Stabilized Soil Pavements. Univ. of California, Berkeley, PhD dissertation, 1968.
4. Troxell, G. E., Raphael, J. M., and Davis, R. E. Long-Time Creep and Shrinkage Tests of Plain and Reinforced Concrete. ASTM Proc., Vol. 58, 1958, pp. 1101-1120.
5. George, K. P. Shrinkage Characteristics of Soil-Cement Mixtures. Highway Research Record 255, 1968, pp. 42-58.
6. Aroni, S., and Mehta, P. K. Fundamentals Underlying Shrinkage in Concrete—A Review. The Indian Concrete Journal, Dec. 1965.
7. Neville, A. M. Properties of Concrete. John Wiley and Sons, New York, 1963.
8. Illson, J. M. The Creep of Concrete Under Uniaxial Tension. Magazine of Concrete Research, Vol. 17, No. 51, June 1965.
9. Meyers, B. L., Slate, F. O., and Winter, G. Relationship Between Time-Dependent Deformation and Microcracking of Plain Concrete. ACI Jour., Vol. 66, No. 1, Jan. 1969, pp. 60-68.
10. Hopkins, I. L., and Hamming, R. W. On Creep and Relaxation. Jour. of Applied Physics, Vol. 28, No. 8, 1957.
11. Monismith, C. L., Alexander, R. L., and Secor, K. E. Rheologic Behavior of Asphalt Concrete. ASTM Proc., Vol. 35, Feb. 1966.
12. Davis, R. E., and Davis, H. E. Flow of Concrete Under Sustained Compressive Stress. ASTM Proc., Part 2, Vol. 30, 1930.
13. Shah, S. P., and Winter, G. Inelastic Behavior and Fracture of Concrete. ACI Jour., Vol. 63, No. 9, Sept. 1966, pp. 925-930.
14. Shah, S. P., and Chandra, S. Critical Stress, Volume Change, and Microcracking of Concrete. ACI Jour., Vol. 65, No. 9, Sept. 1968, pp. 770-781.

15. Davies, J. D., and Bose, D. K. Stress Distribution in Splitting Tests. ACI Jour., Vol. 65, No. 8, Aug. 1968, pp. 662-669.
16. Bresler, B., and Pister, K. S. Failure of Plain Concrete Under Combined Stresses. ASTM Proc., Vol. 81, Sep. No. 674, April 1955.
17. McHenry, D., and Karni, J. Strength of Concrete Under Combined Tensile and Compressive Stresses. ACI Jour., Vol. 54, No. 10, April 1958.
18. Kupfer, H., Hilsdorf, H. K., and Rusch, H. Behavior of Concrete Under Biaxial Stresses. ACI Jour., Vol. 66, No. 8, Aug. 1969, pp. 656-666.
19. Pagen, C. A. An Analysis of the Thermorheological Response of Bituminous Concrete. Eng. Exp. Station, Ohio State Univ., Columbus, PhD dissertation, 1963.
20. Paduana, J. A. The Effect and Amount of Clay on the Strength and Creep Characteristics of Clay-Sand Mixtures. Univ. of California, Berkeley, PhD dissertation, 1966.
21. Kasianchuk, D. A. Fatigue Considerations in the Design of Asphalt Concrete Pavements. Univ. of California, Berkeley, PhD dissertation, 1968.
22. Pretorius, P. C. Design Considerations for Pavements Containing Soil-Cement Bases. Univ. of California, Berkeley, PhD dissertation, 1970.
23. Wilson, E. L. A Digital Computer Program for the Finite Element Analysis of Solids With Non-Linear Material Properties. Dept. of Civil Engineering, Univ. of California, Berkeley.

APPENDIX

AXISYMMETRIC FINITE-ELEMENT ANALYSIS OF SHRINKAGE STRESSES IN PAVEMENTS

The finite-element approach to the determination of shrinkage stresses in a pavement, for 1 increment of time, is briefly summarized in the following.

The potential energy of an elastic solid is given by

$$\phi = \int_{\text{volume}} \tfrac{1}{2}\epsilon_i\sigma_i dV - \int_{\text{volume}} w_i F_i dV - \int_{\text{area}} w_i P_i dA \qquad (1)$$

where

w = displacement of point i in an elastic solid,
F = body force, and
P = surface traction.

Written in matrix form, Eq. 1 becomes

$$\phi = \int_{\text{volume}} \tfrac{1}{2}[\epsilon]^T[\sigma]dV - \int_{\text{volume}} [w]^T[F]dV - \int_{\text{area}} [w]^T[P]dA \qquad (2)$$

For a finite-element system composed of M arbitrary elements, Eq. 2 is written as a sum of integrals (23):

$$\phi = \sum_{m=1}^{M} \left\{ \int_{\text{volume}} \tfrac{1}{2}[\epsilon]^T[\sigma]dV - \int_{\text{volume}} [w]^T[F]dV - \int_{\text{area}} [w]^T[P]dA \right\} \qquad (3)$$

The potential energy is expressed in terms of unknown nodal point displacements by assuming a displacement field within each element, satisfying compatibility between elements of the system

$$[w] = [d]\,[u] \tag{4}$$

where $[u]$ = unknown nodal point displacements. Element strains are expressed as

$$[\epsilon] = [a]\,[u] \tag{5}$$

For an elastic material the stresses are expressed in terms of corresponding strains and environmental effects by the elastic stress-strain relationship

$$[\sigma] = [C]\,[\epsilon] - [\tau] \tag{6}$$

Equations 4, 5, and 6 are substituted into Eq. 3 to result in the following expression for the potential energy:

$$\phi = \sum_{m=1}^{M} \left\{ \tfrac{1}{2} \int_{\text{volume}} [u]^T [a]^T [C] [a] [u]\, dV - \int_{\text{volume}} [u]^T \left([d]^T [F] + [a]^T [\tau] \right) dA - \int_{\text{area}} [u]^T [d]^T [P]\, dA \right\} \tag{7}$$

The potential energy is minimized by the requirement

$$\frac{\delta \phi}{\delta u_i} = 0 \text{ for } i = 1, \ldots, N$$

where N is the number of unknown nodal point displacements.

After matrix differentiation, the equilibrium of the finite-element system is given by

$$\sum_{m=1}^{M} \int_{\text{volume}} [a]^T [C] [a] [u]\, dV = \Sigma \int_{\text{volume}} [d]^T [F] + [a]^T [\tau]\, dV + \Sigma \int_{\text{area}} [d]^T [P]\, dA$$

or

$$[K]\,[u] = [Q] \tag{8}$$

where $[K]$ is the stiffness matrix given by

$$[K] = \sum_{m=1}^{M} [k^m]$$

The individual-element stiffnesses are given by

$$[k^m] = \int_{\text{volume}} [a]^T [C] [a]\, dA$$

The load vector $[Q]$ is defined as

$$[Q] = \sum_{m=1}^{M} \left\{ \int_{\text{volume}} ([d]^T [F] + [a]^T [\tau])\, dV + \int_{\text{area}} [d]^T [P]\, dA \right\} \tag{9}$$

Equation 8 can now be solved for the unknown nodal point displacements $[u]$.

Shrinkage and thermal effects are included in Eq. 6 for the axisymmetric solid as

$$\begin{Bmatrix}\sigma_{rr}\\ \sigma_{zz}\\ \sigma_{\theta\theta}\\ \sigma_{rz}\end{Bmatrix} = \begin{bmatrix}C_{11} & C_{12} & C_{13} & 0\\ C_{21} & C_{22} & C_{23} & 0\\ C_{31} & C_{32} & C_{33} & 0\\ 0 & 0 & 0 & C_{44}\end{bmatrix} \begin{Bmatrix}\epsilon_{rr}\\ \epsilon_{zz}\\ \epsilon_{\theta\theta}\\ \epsilon_{rz}\end{Bmatrix} - \begin{bmatrix}C_{11} & C_{12} & C_{13} & 0\\ C_{21} & C_{22} & C_{23} & 0\\ C_{31} & C_{32} & C_{33} & 0\\ 0 & 0 & 0 & 0\end{bmatrix} \begin{Bmatrix}T\alpha_{tt} + S_{rr}\\ T\alpha_{zz} + S_{xx}\\ T\alpha_{\theta\theta} + S_{\theta\theta}\\ 0\end{Bmatrix} \tag{10}$$

where

T = temperature,
α = coefficient of thermal expansion, and
S = shrinkage strain.

These thermal and shrinkage stresses for the restraint conditions are transformed to nodal point forces by Eq. 9.

The step-by-step time incremental procedure is handled as follows. For a 1-dimensional viscoelastic material subjected to a strain rate, the stress after an elapsed time t is given by

$$\sigma(t) = \int_0^t E(t-\tau)\frac{d\epsilon(\tau)}{d\tau}\,d\tau$$

$$\sigma(t) = \sum_{i=0}^{n-1} \int_{t_i}^{t_{i+1}} E(t-\tau)\frac{d\epsilon(\tau)}{d\tau}\,d\tau$$

If the time increments are made small enough, the trapezoidal rule can be used.

$$\sigma(t_n) = \sum_{i=0}^{n-1} \tfrac{1}{2}\left[E(t_n - t_{i+1}) - E(t_n - t_i)\right]\left[\epsilon(t_{i+1}) - \epsilon(t_i)\right]$$

$$= \sum_{i=0}^{n-1} \left[E(t_n - t_{i+\frac{1}{2}})\right]\left[\epsilon(t_{i+1}) - \epsilon(t_i)\right]$$

For an axisymmetric solid, this equation becomes

$$\begin{Bmatrix}\sigma_{rr}\\ \sigma_{zz}\\ \sigma_{\theta\theta}\\ \sigma_{rz}\end{Bmatrix} = \sum_{i=0}^{n-1} \frac{E(t_n - t_{i+\frac{1}{2}})}{(1+\nu)(1-2\nu)} \begin{bmatrix}1-\nu & \nu & \nu & 0\\ \nu & 1-\nu & \nu & 0\\ \nu & \nu & 1-\nu & 0\\ 0 & 0 & 0 & \frac{1-2\nu}{2}\end{bmatrix} \begin{Bmatrix}\Delta\epsilon_{rr}(t_{i+1})\\ \Delta\epsilon_{zz}(t_{i+1})\\ \Delta\epsilon_{\theta\theta}(t_{i+1})\\ \Delta\epsilon_{rz}(t_{i+1})\end{Bmatrix}$$

where $\Delta\epsilon(t_{i+1}) = \epsilon(t_{i+1}) - \epsilon(t_i)$.